Advances in Concrete Construction, *Vol. 9, No. 3* (*2020*) *313-326*
DOI: https://doi.org/10.12989/acc.2020.9.3.313

Effect of geometrical configuration on seismic behavior of GFRP-RC beam-column joints

Shervin K. Ghomi[a] and Ehab El-Salakawy*

Department of Civil Engineering, University of Manitoba, Winnipeg, Canada

(*Received May 18, 2019, Revised February 14, 2020, Accepted February 17, 2020*)

Abstract. Glass fiber-reinforced polymer (GFRP) bars have been introduced as an effective alternative for the conventional steel reinforcement in concrete structures to mitigate the costly consequences of steel corrosion. However, despite the superior performance of these composite materials in terms of corrosion, the effect of replacing steel reinforcement with GFRP on the seismic performance of concrete structures is not fully covered yet. To address some of the key parameters in the seismic behavior of GFRP-reinforced concrete (RC) structures, two full-scale beam-column joints reinforced with GFRP bars and stirrups were constructed and tested under two phases of loading, each simulating a severe ground motion. The objective was to investigate the effect of damage due to earthquakes on the service and ultimate behavior of GFRP-RC moment-resisting frames. The main parameters under investigation were geometrical configuration (interior or exterior beam-column joint) and joint shear stress. The performance of the specimens was measured in terms of lateral load-drift response, energy dissipation, mode of failure and stress distribution. Moreover, the effect of concrete damage due to earthquake loading on the performance of beam-column joints under service loading was investigated and a modified damage index was proposed to quantify the magnitude of damage in GFRP-RC beam-column joints under dynamic loading. Test results indicated that the geometrical configuration significantly affects the level of concrete damage and energy dissipation. Moreover, the level of residual damage in GFRP-RC beam-column joints after undergoing lateral displacements was related to reinforcement ratio of the main beams.

Keywords: GFRP-RC; seismic performance; cyclic loading; beam-column joints; reinforcement ratio; latera load-drift response; interior beam-column joints; exterior beam-columns; damage index

1. Introduction

Beam-column joints are key elements in defining seismic behavior of moment-resisting frames in terms of lateral stiffness and energy dissipation. Moreover, failure of these elements during an earthquake can lead to partial or even total failure of the structure. Steel-reinforced concrete (RC) moment-resisting frames are considered as one of the main lateral load-resisting systems in buildings. Therefore, various parameters affecting the seismic behavior of steel-RC beam-column joints have been extensively studied (Hanson and Connor 1967, Paulay *et al*. 1978, Ehsani and Wight 1985, Kim and LaFave 2007, Le-Trung *et al*. 2013).

However, combining or fully replacing the steel reinforcement with alternative materials may be undertaken by structural designers to achieve superior performance in specific aspects, which can affect the behavior of moment-resisting frames. For example, fiber-reinforced polymers (FRPs) are used as external reinforcement in forms of laminates and wraps to strengthen existing steel-RC structures (Mirmiran and Shahawy 1997, Pessiki *et al*. 2001, Esfandiari and Esfandiari 2016, Kakaletsis 2016, Sumathi and Vignesh 2017, Karayannis and Golias 2018, Esfandiari and Soleimani 2018) or as an effective alternative for internal steel reinforcement to improve the performance of new RC structures in terms of corrosion resistance, especially in harsh environments (Brown and Bartholimew 1993, Tobbi *et al*. 2012, Tobbi *et al*. 2014, Ju *et al*. 2017, Guerin *et al*. 2018). However, the possible effects that FRP reinforcement can have on the seismic performance of moment-resisting frames, is not fully understood yet.

Recently, some studies have investigated the seismic behavior of RC beams (Liang *et al*. 2016), columns (Tavassoli *et al*. 2015, Tavassoli and Sheikh 2017, Esfandiari and Latifi 2019) and beam-column joints (Said and Nehdi 2004, Mady *et al*. 2011, Sharbatdar *et al*. 2011, Ghomi and El-Salakawy 2016, Hasaballa and El-Salakawy 2016) internally reinforced with FRP materials. Among various types of FRP materials commonly available in the construction industry, Glass FRP (GFRP) is considered the most suitable option for seismic design (Ghomi and El-Salakawy 2016, Hasaballa and El-Salakawy 2016). This is due to the relatively high tensile strength and low modulus of elasticity of GFRP materials that allows them to withstand significantly large deformations prior to rupture. This characteristic, so-called "deformability", compensates for the lack of ductility in FRP-RC structures caused by the linear elastic stress-strain relationship of FRP material without any yielding (as oppose to conventional steel reinforcement).

*Corresponding author, Professor
E-mail: ehab.el-salakawy@umanitoba.ca
[a]PhD Candidate
E-mail: khalilis@myumanitoba.ca

 ISSN: 2287-5301 (Print), 2287-531X (Online)

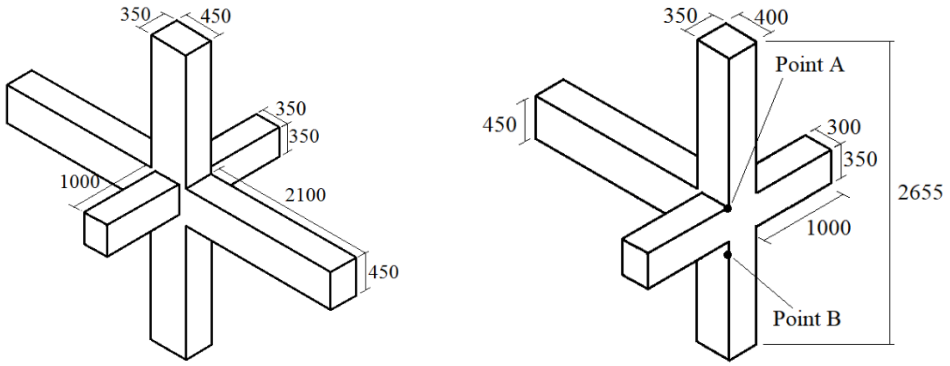

(a) Interior beam-column joint (b) Exterior beam-column joint

Fig. 1 Dimensions of test specimens (dimensions in mm)

Despite the early studies on various key parameters of the seismic behavior of GFRP-RC beam-column joints such as type of reinforcement, joint shear stress, presence of lateral beams, reinforcement detailing and concrete strength (Said and Nehdi 2004, Mady *et al*. 2011, Ghomi and El-Salakawy 2016, Hasaballa and El-Salakawy 2016), there are still many parameters affecting the behavior of GFRP-RC beam-column joints that are not fully explored.

For example, although the effect of joints' geometrical configuration (interior and exterior connections) has been established for steel-RC joints (ACI 2002), up to date, no clear comparison between the seismic behavior of interior and exterior GFRP-RC beam-column joints has been performed. Therefore, in the current program, the effect of geometrical configuration on the seismic performance of GFRP-RC beam-column joints is investigated.

Ghomi and El-Salakawy (2016) and Hasaballa and El-Salakawy (2016) studied the seismic behavior of various exterior GFRP-RC beam-column joints and observed that well-designed GFRP-RC beam-column joints can withstand lateral drift ratios as high as 9% without exhibiting brittle failure. Since 9% lateral drift ratio is much more than what is generally expected from a beam-column joint in a regular moment-resisting frame, it was concluded that GFRP-RC elements can be used in seismic regions.

Moreover, the authors concluded that, due to the linear elastic nature of GFRP materials, exterior GFRP-RC beam-column joints exhibit significantly lower residual damage after a seismic event compared to steel-RC counterparts. This feature can significantly reduce the cost of repair or eliminate the need for demolishing the structure after an earthquake event.

However, following an earthquake, the service and ultimate performance of a GFRP-RC moment-resisting frame has to be determined to assess the ability of the structure to remain in service. Therefore, the magnitude of damage and its effect on GFRP-RC moment frames, under reversed-cyclic loading must be investigated.

To address this gap, two full-scale GFRP-RC beam-columns joints were constructed and tested under multiple reversal loading schemes. The magnitude of damage, energy dissipation, mode of failure and stress distribution at various loading stages were investigated. Moreover, the performance of the specimens under service loading after surviving various intensity of earthquake loadings was studied.

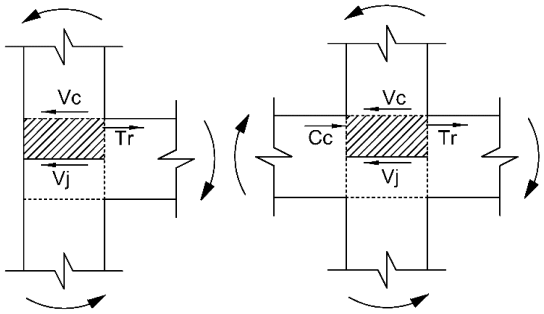

Fig. 2 Free-body diagrams to calculate shear force at mid-height of joints

Although several quantitative measures of deterioration of steel-RC structures under reversal loadings have been proposed in the literature, up to date, no model has been developed to quantify the magnitude of damage in GFRP-RC elements. Therefore, in the current program, a modified damage index based on the model proposed by Park and Ang (1985) is proposed as a tool to measure the magnitude of damage in GFRP-RC beam-column joints under dynamic loadings.

2. Experimental program

2.1 Test specimens

Two full-scale GFRP-RC beam-column joints were constructed and tested under quasi-static reversal cyclic loading. Fig. 1 shows dimension of the specimens. Height of the columns and length of the beams were 2,655 and 2,100 mm, respectively. Dimensions of the lateral beams were proportioned to cover approximately 60% of the joint area. Both specimens were designed to have a maximum joint shear stress of $1.3\sqrt{f'_c}$.

The maximum joint shear stress in the specimens was calculated at middle-height of the joint area according to the free-body diagrams (hatched areas) shown in Fig. 2. In Fig. 2, V_j indicates the shear force at mid-height of the joint, T_r indicates tensile force applied to the joint by the

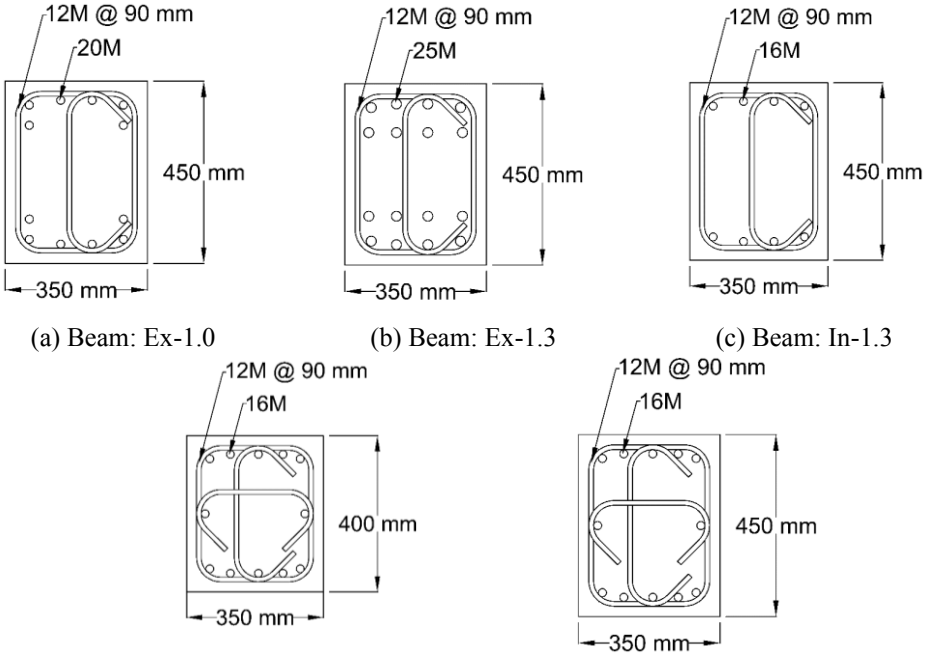

(a) Beam: Ex-1.0 (b) Beam: Ex-1.3 (c) Beam: In-1.3

(d) Column: exterior joint (e) Column: interior joint

Fig. 3 Reinforcement detailing of test specimens

Table 1 Specimens' properties

Specimen	Beam Reinforcement (Top and Bottom)	Beam Flexural Capacity (kN.m)	Column Flexural Capacity (kN.m)	Flexural Ratio	Joint Shear Ratio	Concrete Strength f'_c (MPa)	Reinforcement Ratio of Beam
Ex-1.0*	6-20M	352	254	1.45	0.96	47	1.34%
Ex-1.3	8-25M	454	262	1.15	1.29	49	3.05%
In-1.3	4-16M	264	280	1.06	1.30	38	0.57%

*Previously tested by the authors (Ghomi and El-Salakawy 2016)

longitudinal reinforcement in the main beam, C_c indicates compressive force applied to the joint by the concrete compressive block and V_c indicates the shear force applied to the joint by the column.

One of the main parameters previously studied by the authors (Ghomi and El-Salakawy 2016) was joint shear stress in exterior beam-column joints. The authors attempted to introduce a joint shear stress limit as the allowable stress in exterior GFRP-RC beam-column joints. The authors tested three full-scale exterior beam-column joints with joint shear stresses of $0.85\sqrt{f'_c}$, $1.0\sqrt{f'_c}$ and $1.1\sqrt{f'_c}$. Test results indicated that GFRP-RC exterior beam-column joints can withstand all three levels of joint shear stress tested. Therefore, it remains unknown that whether such beam-column joints can withstand higher levels of joint shear stresses or not. Therefore, in this program, the joint shear stress of $1.3\sqrt{f'_c}$ was selected as the baseline for the design of test specimens.

The results obtained from testing the exterior specimen with joint shear stress of $1.3\sqrt{f'_c}$ is compared to the findings of Ghomi and El-Salakawy (2016) from testing an exterior GFRP-RC beam-column joint with the same dimensions but different number of longitudinal bars in the main beam, which resulted in a different level of joint shear stress $1.0\sqrt{f'_c}$.

The specimens presented in this document are designated with a two-part name, the first part indicating the type of connection ("Ex" for exterior beam-column joints and "In" for interior beam-column joint) and the second part indicating the level of joint shear stress ("1.0" for joint shear stress of $1.0\sqrt{f'_c}$ and "1.3" for joint shear stress of $1.3\sqrt{f'_c}$). Reinforcement detailing of the test specimens, In-1.3 and Ex-1.3, and the beam-column joint previously tested by Ghomi and El-Salakawy (2016), Ex-1.0, are shown in Fig. 3.

Table 1 shows the properties of test specimens based on the compressive strength of concrete on the day of testing. In the exterior specimens, the longitudinal reinforcement of the beam was bent into the column to provide sufficient anchorage.

The value of "Flexural Ratio" in Table 1 indicates the ratio of the sum of flexural strength of columns (including the axial load effect) over the sum of flexural strength of beams in each specimen.

2.2 Material

Ready-mix concrete with target 28-day compressive strength of 40 MPa was used to cast the test specimens. The actual concrete compressive strength was measured through standard compressive test of 150×300 mm cylinders. The

Table 2 Reinforcement properties

Reinforcement Type	Tensile Strength (MPa)	Modulus of Elasticity (GPa)	Ultimate Tensile Strain (micro-strain)	Area (mm^2)
Straight Bars	1,184	62.6	18,900	198
Bent Bars*	992	50.0	19,850	507
Stirrups and Ties*	1,022	50.0	20,450	71

*Properties provided in the table are corresponding to the straight portion of the bar

Fig. 4 Test set-up

concrete compressive strength of each specimen on the day of testing is presented in Table 1.

Sand-coated GFRP bars and stirrups were used to reinforce the test specimens in the current program (Ex-1.3 and In.1.3). The mechanical properties of the reinforcement, as provided by the manufacturer (Pultrall Inc. 2019), are presented in Table 2. As mentioned earlier, bent bars were used to anchor longitudinal bars of the main beam into the joint area of Specimen Ex-1.3. The ultimate tensile strength and modulus of elasticity of the longitudinal bars in the main beam of Specimen Ex-1.0 were reported by the manufacturer (Schoeck Canada Inc. 2019) as 850 MPa and 50 GPa, respectively. Details of the mechanical properties of the reinforcement of Specimen Ex-1.0 are provided elsewhere (Ghomi and El-Salakawy 2016).

2.3 Test set-up

The specimens were tested while the columns and the beams were in vertical and horizontal position, respectively (Fig. 4). The specimens were isolated from the assumed points of zero-moments in an arbitrary moment-resisting frame. Therefore, a roller and a pin boundary condition was simulated in the test set-up at tips of the beams and bottom of the columns, respectively.

The roller boundary condition was simulated by means of a link (double-hinged element). The links were connecting the tips of the beams to the laboratory strong floor. The pin boundary condition was simulated by means of a hinge at the bottom of the column. Similar to the links, the hinge was also attached to the strong floor by the pre-stressing force of four Dywidag bars.

A fully dynamic 1000-kN capacity actuator was mounted on a strong concrete wall and was attached to upper tip of the column to apply reversal cyclic loading to simulate a seismic event. the columns were also under constant axial load during the test by means of a hydraulic

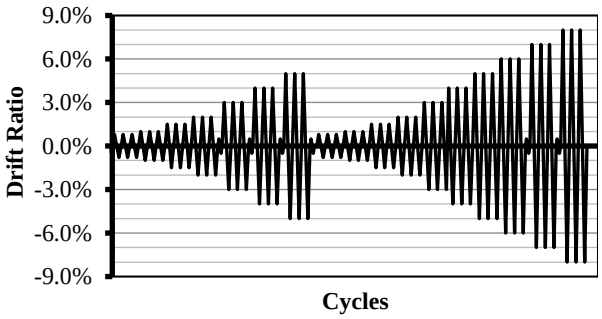

Fig. 5 Loading scheme

jack reacting against a stiff steel beam on top of the specimens. The stiff steel beam was connected to the strong floor by means of two double-hinged elements to allow for its free movement while the actuator applies reversal loadings to the column by pivoting about the axis of the pin in the bottom hinge.

Therefore, the line of action of the column axial load always passed through the center of the pin of the hinge at the bottom of the column. This was done to eliminate secondary moments in the column due to the distance between center of gravity of the column and the line of action of the axial load.

2.4 Loading scheme

Fig. 5 shows the loading scheme that was used to test the specimens in this program. The general scheme of the loading procedure was in displacement-controlled mode and was obtained from the ACI 374.1-05 report (ACI Committee 374 2005).

In this program, the specimens were tested under two loading phases. In the first phase, the specimen was tested according to a loading scheme that simulated a severe earthquake up to 5% drift ratio. Then the specimen was re-loaded up to failure following the same loading scheme in the second loading phase to study their performance in ultimate loading state after surviving an earthquake.

Based on orientation of the specimens in the test set-up that was used in this program, the lateral drift ratio was defined as the ratio of column tip displacement to column height.

The loading scheme consisted of several loading steps gradually increasing in lateral drift ratio. Each loading step included three identical loading cycles. After 2% drift ratio, one load-controlled cycle with an amplitude equal to service load was applied after each loading step. The service load condition was defined as the load corresponding to 25% of the ultimate strain capacity of the longitudinal GFRP bars in the beams.

3. Test results and discussions

3.1 Lateral load-drift response

The relationship between the load at tip of the column (actuator load) and the lateral drift ratio (hysteresis

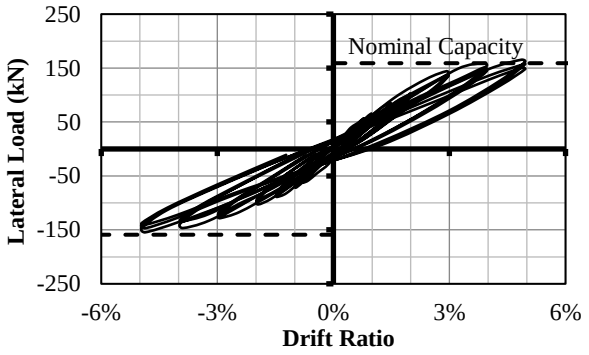

(a) Specimen Ex-1.3

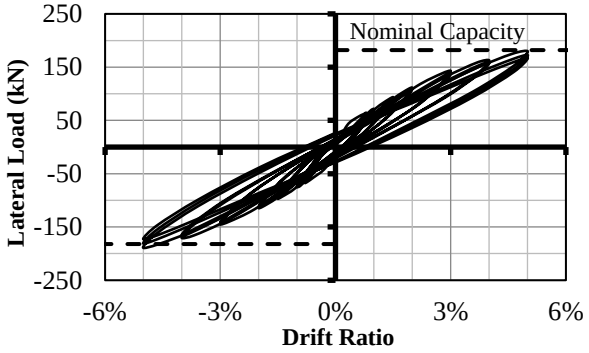

(b) Specimen In-1.3

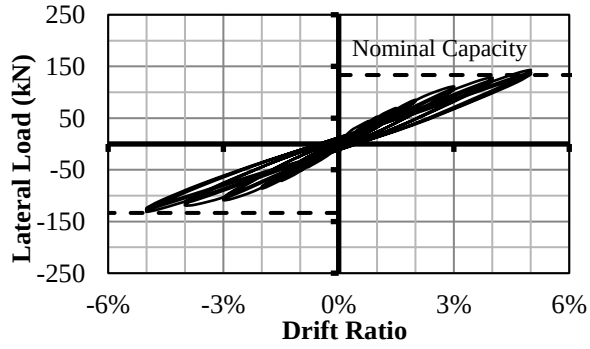

(c) Specimen Ex-1.0

Fig. 6 Lateral load-drift response of test specimens during the first loading phase

diagram) of the test specimens are shown in Figs. 6(a) and 6(b). Moreover, the column lateral load-drift response corresponding to the exterior beam-column joint with joint shear ratio of $1.0\sqrt{f'_c}$, previously tested by the authors (Ghomi and El-Salakawy 2016) is shown in Fig. 6(c) for comparison. The dashed lines in the hysteresis diagrams show the nominal capacity of the specimens, defined as the column lateral load that results in the maximum nominal bending moment in the main beams.

It should be mentioned that, the test set-up used to test Specimen Ex-1.0 was different from the set-up used to test the specimens in the present program (Specimen Ex-1.3 and Specimen In-1.3). Details of the test set-up used for testing Specimen Ex-1.0 are presented elsewhere (Ghomi and El-Salakawy 2016). However, it should be mentioned that despite the different test set-ups, the same loading configuration was applied to all specimens included in this paper; therefore, the results are comparable.

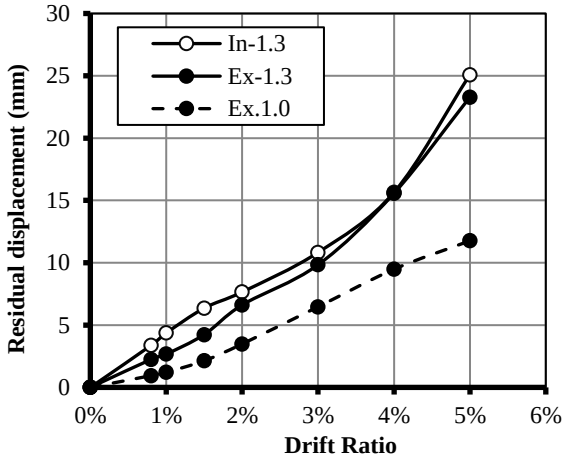

Fig. 7 Residual displacement of tip of columns during the first loading phase

Comparing the hysteresis diagram of interior and exterior specimens indicates asymmetric behavior of the exterior beam-column joints compared to the interior one. Specimen In-1.3 showed very similar behavior in both negative and positive direction. This is evident by the fact that the specimen reached its nominal capacity at 5% drift ratio in both positive and negative direction.

The exterior specimens (Ex-1.0 and Ex-1.3), on the other hand, showed slightly higher stiffness during loading in the positive direction than the negative direction. The specimens reached their nominal capacity at 4% and 5% drift ratios in positive and negative directions, respectively. This could be due to asymmetric geometry of the exterior beam-column joints. As shown in Fig. 1, centerline of the lateral beams in the exterior beam-column joints does not coincide with center point of the joint as the lateral beams are flush with the backside of the column and topside of the main beam. With this configuration, Point A is confined by lateral beams, while there was no confinement at Point B (Fig. 1). Therefore, the concrete near Point A provided higher compressive resistance compared to the concrete near Point B. Consequently, the test specimens showed higher lateral load carrying capacity when the column was pushed toward the positive direction (Point A in compression) and lower capacity when the columns were pulled toward the negative direction (Point B in compression). The interior specimen; however, due to symmetrical geometry with respect to centerline of the column, exhibited similar behavior in both positive and negative direction.

By reaching its maximum bending capacity, the main beam in Specimen Ex-1.3 exerted a joint shear stress of $1.3\sqrt{f'_c}$ (as shown in Table 1). Therefore, it can be concluded that GFRP-RC exterior beam-column joints with the geometrical configuration tested in this program are able to withstand joint shear stress of $1.3\sqrt{f'_c}$.

All specimens were able to reach their nominal capacity prior to 5% drift ratio without exhibiting significant concrete damage. However, the magnitude of observed residual displacement varied among the specimens. Fig. 7 shows residual displacement of the specimens at tip of the

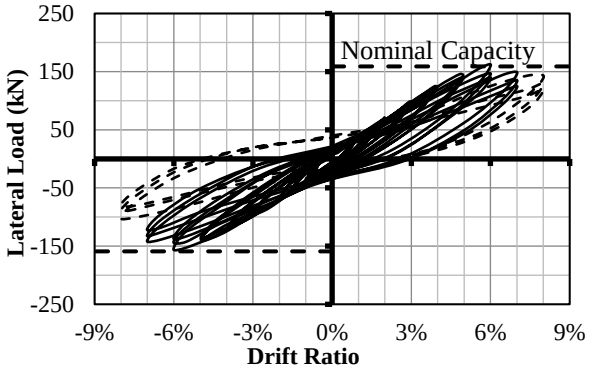

(a) Specimen Ex-1.3

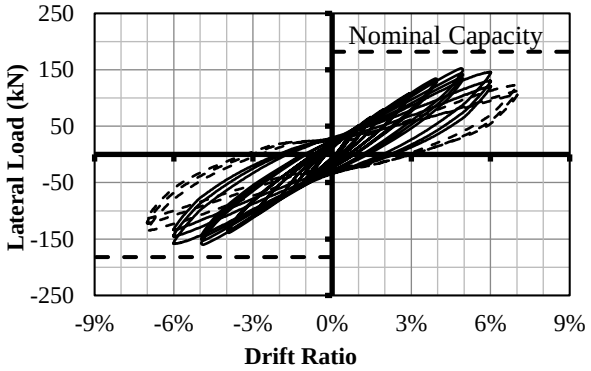

(b) Specimen In-1.3

Fig. 8 Lateral load-drift response of test specimens during the second loading phase

columns after each loading step during the first loading phase. The residual displacement was measured at the point of zero lateral load.

As indicated in Fig. 7, the increase in joint shear stress of exterior beam-column joints increased the magnitude of residual damage. This is due to higher concrete damage induced to the joint area because of higher joint shear stresses. This can be also observed in the hysteresis diagrams by wider loops in response of Specimen Ex-1.3 compared to that of Specimen Ex-1.0.

In general, Specimen In-1.3 showed slightly more residual deformation compared to Specimen Ex-1.3, with the same level of joint shear stress. That could be attributed to the fact that Specimen In-1.3 contained more concrete volume compared to Specimen Ex-1.3, which resulted in more areas that inelastic deformation due to concrete damage (cracks) occurred.

As mentioned earlier, the beam-column joints in the current program were tested under a two-phase loading scheme. Fig. 8 shows hysteresis diagram of Specimens In-1.3 and Ex-1.3 during the second loading phase. The hysteresis loops of the last loading step (failure) is shown with dashed lines in Fig. 8.

As expected, the specimens showed linear behavior up to 5% drift ratio during the second loading phase. Specimen Ex-1.3 and In-1.3 reached their maximum lateral load during the second loading phase at 6% and 5% lateral drift ratio, respectively. Both specimens exhibited gradual decrease in lateral load carrying capacity after reaching the

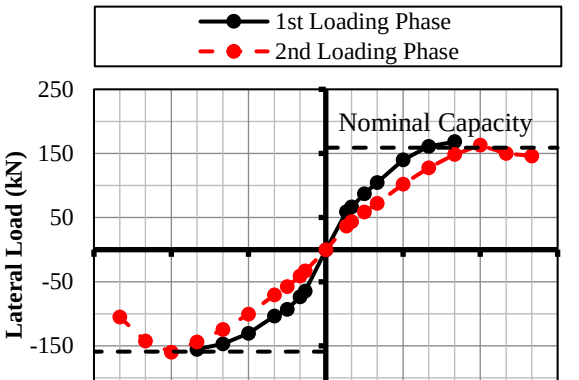

(a) Specimen Ex-1.3

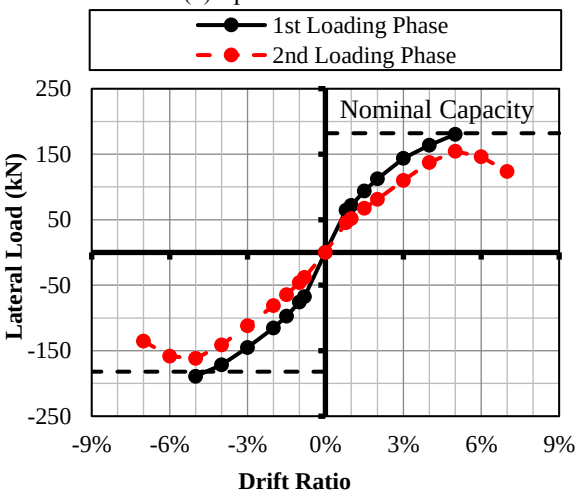

(b) Specimen In-1.3

Fig. 9 Lateral load envelope of test specimens during the first and the second loading phase

maximum lateral load during the second loading phase until the failure was observed in the specimens (8% and 7% in Specimen Ex-1.3 and In-1.3, respectively).

According to ACI 374.1-05 (ACI 2005), the failure was defined as the stage at which the lateral load carrying capacity of the specimens decreased less than 75% of the maximum lateral load.

Fig. 9 compares lateral load envelopes of Specimens In-1.3 and Ex-1.3 during the first and the second loading phase. The linear behavior of the specimens during the second loading phase up to 5% drift ratio is indicated by a straight line connecting the origin to the maximum lateral load that the specimens obtained during the third cycle of the 5% drift ratio-loading step in the first loading phase.

Specimen Ex-1.3 was able to reach its nominal capacity during the second loading phase while Specimen In-1.3 with the same magnitude of joint shear stress only reached 85% and 89% of the nominal capacity in positive and negative direction during the second loading phase, respectively. However, this observation was opposite to what was expected. In general, the interior beam-column joint was expected to exhibit less loss in lateral load

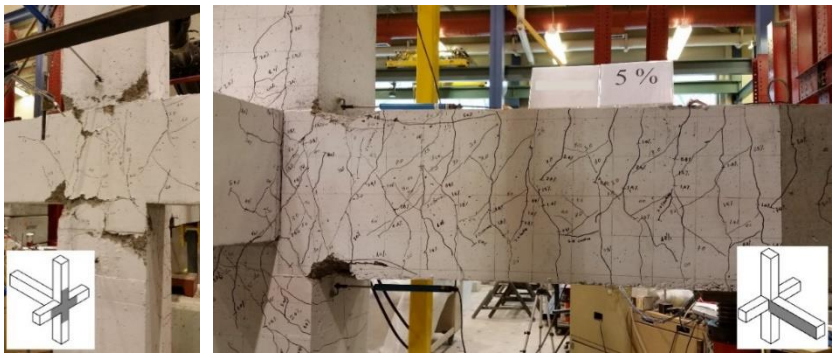

(a) Specimen Ex-1.3

(b) Specimen In-1.3

Fig. 10 Condition of test specimens at the end of the first loading phase

(a) Specimen Ex-1.3

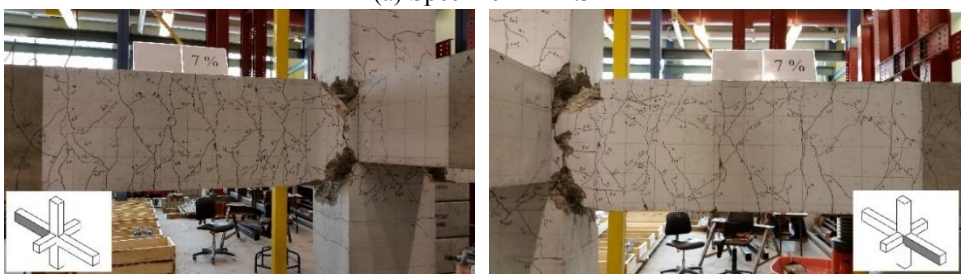

(b) Specimen In-1.3

Fig. 11 Condition of test specimens at failure

carrying capacity compared to the exterior beam-column joint because of more confinement provided to the joint area from the main beams on each side of the joint.

However, the authors believe the main reason for the better performance of Specimen Ex-1.3 compared to Specimen In-1.3 during the second loading phase is the more confinement in the main beams provided by the longitudinal reinforcement. As shown in Fig. 3, the main beam in Specimen Ex-1.3 were heavily reinforced with two layers of 25M bars, while the beams in Specimen In-1.3 were only reinforced with one layer of reinforcement. Thus, less confinement was provided to the concrete core in the main beams of Specimen In-1.3. This resulted in more concrete damage in the main beams, which led to more loss in the lateral load carrying capacity in Specimen In-1.3 compared to Specimen Ex-1.3.

3.2 Mode of failure

Fig. 10 shows the condition of the test specimens at the

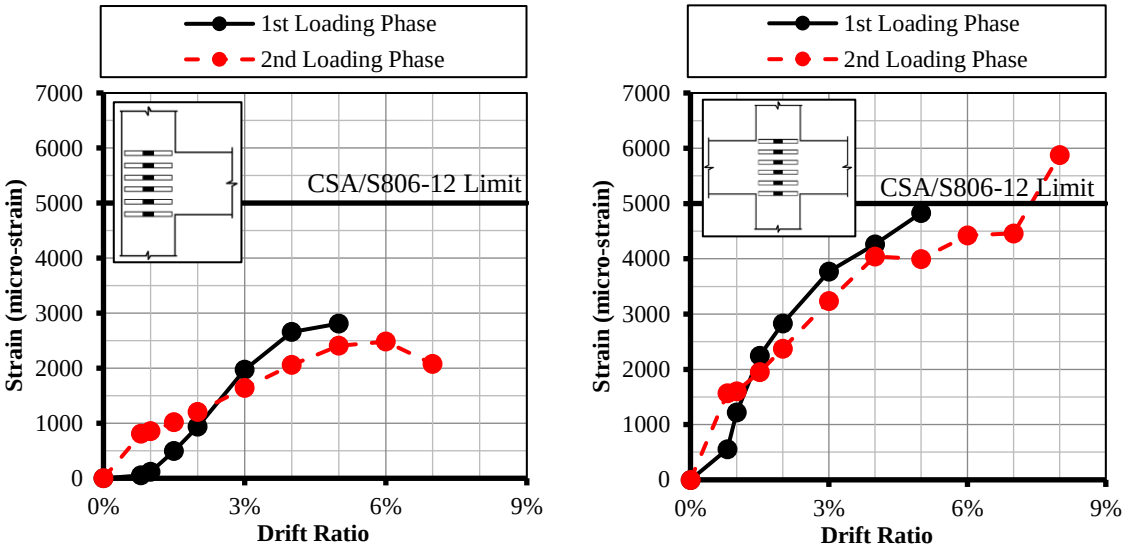

(a) Specimen In-1.3 (b) Specimen Ex-1.3

Fig. 12 The maximum strains in joint stirrups

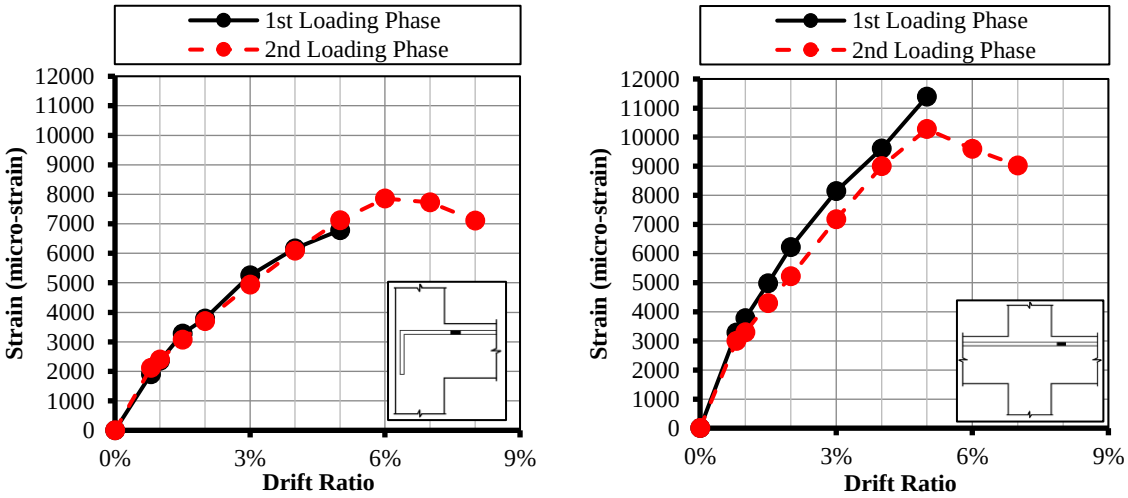

(a) Specimen Ex-1.3 (b) Specimen In-1.3

Fig. 13 The maximum strains in longitudinal bars of beams

end of the first loading phase (5% drift ratio). As shown in the figure, in both specimens, concrete damage was only limited to concrete cover spalling in the main beam adjacent to the column. Since the GFRP-RC beam-column joints were designed as over-reinforced sections (failure occurs due to crushing of concrete), the concrete cover spalling observed in the beams was indicating that maximum bending moment capacity of the beam section was reached.

Fig. 11 shows condition of Specimens In-1.3 and Ex-1.3 at failure during the second loading phase. As shown in the pictures, Specimen Ex-1.3 exhibited severe concrete damage in the joint area, while the joint in Specimen In-1.3 with the same amount of joint shear stress remained intact. This was due to the additional confinement provided to the joint area by the main beams on the opposite sides of the joint in the interior specimen, which increased concrete strength in the joint area and reduced the damage.

However, as shown in the hysteresis diagrams of specimens, both specimens failed due to gradual decrease in lateral load carrying capacity without exhibiting any brittle failure or sudden rupture of the GFRP reinforcement. This was due to the significant reserve of strain in the longitudinal bars of the main beams (difference between measured strain and strain capacity). The authors concluded that providing this methodology in designing GFRP-RC sections can prevent brittle failure of GFRP-RC moment-resisting frames during an earthquake.

3.3 Strain-drift response

The specimens were well instrumented with electrical strain gauges installed on the internal GFRP reinforcement in various locations including 6 gauges on transverse reinforcement (stirrups) in the joint area. Fig. 12 shows the

maximum strain obtained from those strain gauges at each drift ratio.

Although both Specimens Ex-1.3 and In-1.3 were designed with the same maximum joint shear stress, it can be seen from the graphs in Fig. 12 that the maximum measured strain in the joint stirrups of Specimen In-1.3 were significantly lower than those in Specimen Ex-1.3. This indicates more concrete damage in the joint of Specimen Ex-1.3 due to less confinement (as explained earlier), which increased shear stresses in the joint stirrups.

The solid horizontal lines in the graphs of Fig. 12 indicate the maximum allowable strain in FRP stirrups according to CSA/S806-12 (CSA 2017). As shown in the graphs, this limit was not exceeded in any of the specimens except at 7% drift
ratio (failure) in Specimen Ex-1.3. As shown in Fig. 11, Specimen Ex-1.3 exhibited significant concrete damage in the joint area, which resulted in excessive stresses in the joint stirrups. However, it should be mentioned that 7% drift ratio is beyond the expected drift ratios of buildings during an earthquake. National Building Code of Canada (NRCC 2015) requires limiting the maximum lateral drift ratio of buildings to 2.5%. Therefore, it can be assumed that the maximum strain in joint stirrups will not exceed the limit set by CSA/S806-12 (CSA 2017) during the expected response range of GFRP-RC buildings to earthquakes.

Fig. 13 shows the maximum strain observed in the longitudinal bars of the main beams at the column face. Strains recorded from Specimen In-1.3 were significantly higher than those recorded from Specimen Ex-1.3. This was due to the higher reinforcement ratio in Specimen Ex-1.3 than Specimen In-1.3. The effect of reinforcement ratio on the maximum expected strain in the longitudinal bars of the main beams will be discussed in the following section. As shown in Table 1, the reinforcement ratio of Specimens In-1.3 was lower than that of Specimen Ex-1.3 (0.57% and 3.05%, respectively).

3.4 Effect of reinforcement ratio on maximum tensile strain in longitudinal bars

The maximum expected strain in longitudinal bars of a given GFRP-RC section has direct relationship with the reinforcement ratio. As explained earlier, it is desirable to maintain a margin between the maximum expected tensile strain in GFRP longitudinal reinforcement and their maximum tensile strain capacity.

The effect of reinforcement ratio on the maximum bar strain in an arbitrary section (shown as a thumbnail) is illustrated in Fig. 14. In the schematic drawing of the arbitrary section, A_s is the area of tensile reinforcement. The same reinforcement properties as those of Specimen Ex-1.3 and In-1.3 were used in producing Fig. 14. According to CSA/S806-12 (CSA 2017), GFRP-RC beams should be designed as over-reinforced sections with provided reinforcement ratios more than the balanced ones (the reinforcement ratio corresponding to simultaneous compressive failure of outer most concrete fiber and tensile failure of outer most reinforcement layer).

It should be mentioned that the values in Fig. 14 were

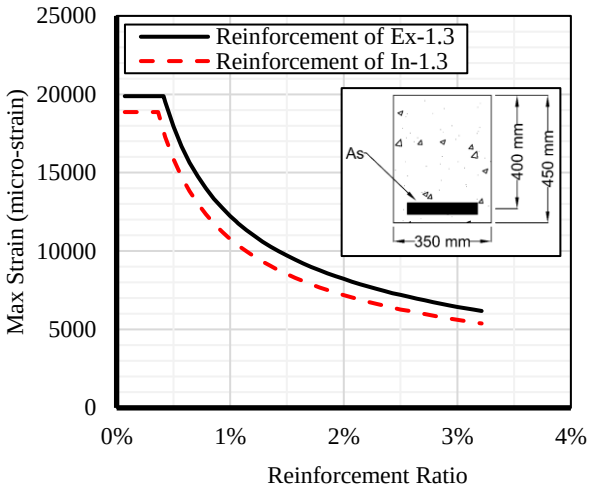

Fig. 14 Effect of reinforcement ratio on maximum strain in longitudinal bars

calculated as strains in longitudinal bars when the strain at the outermost fiber of the concrete reaches 3,500 micro-strain, the ultimate compressive strain of concrete according to CSA/A.23-14 (CSA 2014). However, as discussed earlier, the concrete section may continue its lateral load carrying further after this stage and exhibit higher strains in the longitudinal reinforcement due to confinement of the concrete core. The effect of such over-strength is not included in Fig. 14.

The balanced reinforcement ratio for the cross-section under consideration (Fig. 14) was calculated as 0.41% and 0.36% for reinforcement properties corresponding to Specimens Ex-1.3 and In-1.3, respectively. Therefore, reinforcement ratios lower than that limit resulted in failure of the section due to bar rupture. This is shown in Fig. 14 as a straight line with value of 19,850 micro-strain and 18,900 micro-strain for Specimen Ex-1.3 and In-1.3, respectively.

As shown earlier in Fig. 13, Specimen Ex-1.3 and In-1.3 had a reserve of 60% and 40% of their ultimate tensile strain capacity compared to the maximum measured tensile strain in the bars and no bar rupture was observed. Therefore, it was concluded that a margin of 40% of the ultimate tensile strain capacity between the maximum expected tensile strain of the longitudinal bars and their ultimate strain capacity may be sufficient to prevent brittle failure of GFRP bars in beams. Therefore, a threshold of 60% of the ultimate tensile strain capacity for GFRP bars is suggested to be maintained when designing GFRP-RC beam-column joints in seismic regions.

To provide 60% threshold in the arbitrary section under consideration (Fig. 14), reinforcement ratios more than 1.05% and 0.91% should be provided in the section with the reinforcement properties of Specimen Ex-1.3 and In-1.3, respectively. These reinforcement ratios are approximately 2.5 times more than the balanced reinforcement ratio that is required by CSA/S806-12 (CSA 2017) (0.41% and 0.36% for Specimen Ex-1.3 and In-1.3, respectively). The same methodology can be used by designers to reduce the risk of brittle failure of GFRP-RC elements during an earthquake event.

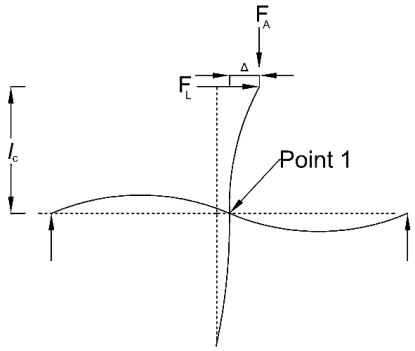

Fig. 15 Effect of reinforcement ratio on maximum strain in longitudinal bars

3.5 Effect of secondary moments

As mentioned earlier, the test set-up used in this program eliminated the effect of secondary moments on the behavior of the specimens. However, secondary moments induced to columns due to lateral movement of frames can significantly increase the magnitude of moments applied to the columns. This can result in premature failure of the columns and collapse of the moment-resisting frames during an earthquake.

To take into account the effect of secondary moments on the test specimens, the additional moment applied to the columns due to lateral displacements were calculated based on the free-body diagram shown in Fig. 15. Total bending moment applied to the columns at Point 1, if the line of action of the axial load applied to the columns were kept vertical during the test (which is the case in a real structure during an earthquake), is calculated as

$$F_L \times l_c + F_A \times \Delta \quad (1)$$

Where F_L is the lateral load applied by the actuator to the upper tip of the column, l_c is the distance between the upper face of the main beams and the centre-line of the actuator, F_A is the axial load applied to the column and Δ is the lateral displacement of the column with respect to the joint.

Fig. 16 compares the maximum bending moments in columns (at top of the joint area, Point 1) of the specimens at each drift ratio with and without considering the secondary bending moments.

As shown in the graphs, including the effect of secondary moments significantly increases the moment applied to the columns at higher drift ratios (19 and 18% at 5% drift ratio in Specimen Ex-1.3 and In-1.3, respectively). Even though none of the test specimens exceeded the bending moment capacity of the columns up to 5% drift ratio (the first loading phase) in the experiment, the graphs indicate that including the effect of secondary moments would result in the column capacities to be exceeded at 4% drift ratio. This could result in premature failure of the moment-resisting frames during an earthquake. Therefore, in this case, the lateral drift ratio of the frame should be limited to 4% drift ratio.

It should be mentioned that the graphs in Fig. 16 were developed based on the axial load applied to the specimen

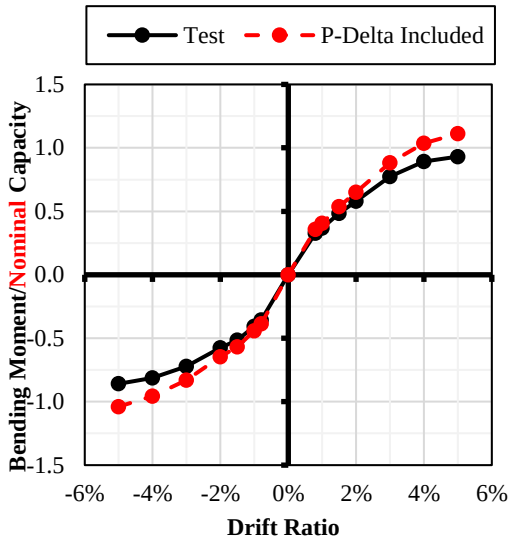

(a) Specimen Ex-1.3

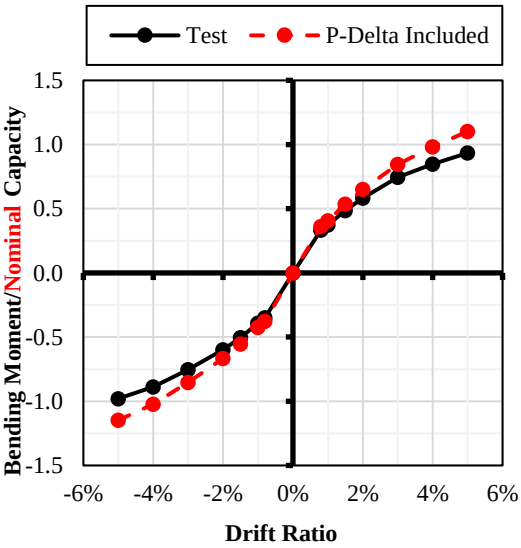

(b) Specimen In-1.3

Fig. 16 Effect of secondary moments on bending moments of columns

during testing. The magnitude of axial loads on columns could vary based on their location in the building and level of service load. However, the same procedure can be followed to obtain an appropriate limit for the lateral drift ratio of a moment-resisting frame.

3.6 Energy dissipation and magnitude of damage

The amount of energy dissipated by the specimen during a specific loading cycle was calculated as the area enclosed by loops corresponding to that loading cycle in the lateral load-displacement diagram. Fig. 17 compares the cumulative energy dissipation of the test specimens.

As shown in Fig. 17, both specimens showed very similar behavior in terms of energy dissipation during the first and the second loading phases. Comparing the graphs indicates that the interior specimen (In-1.3) showed higher energy dissipation compared to the exterior one (Ex-1.3).

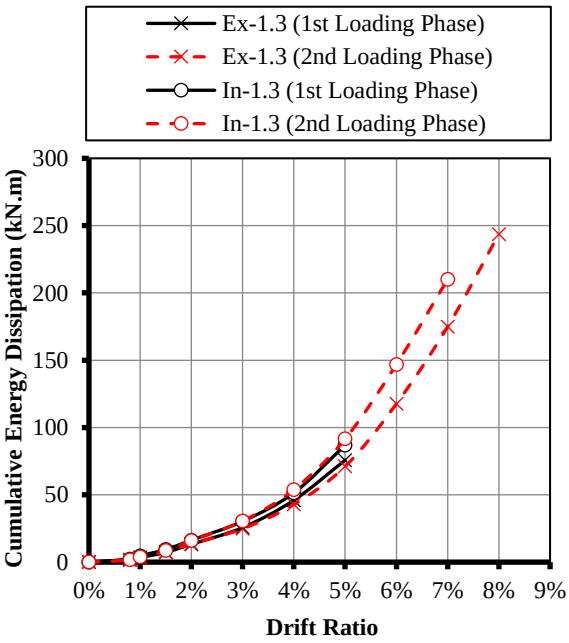

Fig. 17 Cumulative energy dissipation of test specimens

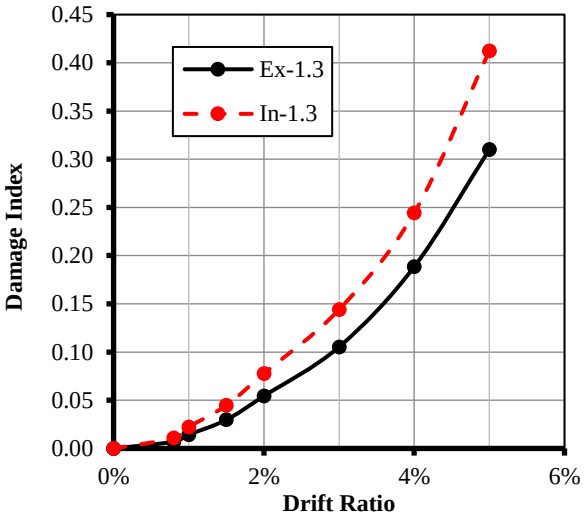

Fig. 18 Damage index-drift ratio

This was expected due to the more residual damage in the interior specimen compared to the exterior one, as discussed earlier. The larger amount of concrete in Specimen In-1.3 increases the area of damaged concrete (crushed or cracked). Since GFRP bars do not yield, the main source of energy dissipation in GFRP-RC frames is limited to concrete damage and slippage of the reinforcement.

Previously, the magnitude of residual deformation was introduced as an indication of the damage level in the test specimens. However, it seems appropriate to adapt a quantitative measurement in terms of damage index to compare the performance of GFRP-RC beam-column joints in terms of magnitude of damage. Park and Ang (1985) have introduced a damage index defined as the linear summation of the damage caused by excessive deformation and the damage caused by repeated cyclic loading effect

$$D = \frac{\delta_{Mx}}{\delta_u} + \frac{\beta}{Q_y . \delta_u} \int dE \tag{2}$$

where, δ_{Mx} is the maximum deformation under earthquake loading; δ_u is the ultimate deflection under monotonic loading; Q_y is calculated yield strength; dE is incremental absorbed hysteric energy and β is a model parameter.

However, due to the linear-elastic nature of GFRP materials, the ductility factor (defined as the ratio of the ultimate deflection over the deflection at design capacity) for GFRP-RC elements is generally lower than their steel-RC counterparts. Therefore, the expression in the damage index corresponding to the excessive damage may not properly reflect the behavior of GFRP-RC beam-column joints.

Since the energy dissipation of GFRP-RC beam-columns are dominantly governed by the magnitude of concrete damage, the authors propose a modified damage index only related to the cumulative energy dissipation of GFRP-RC beam-column joints as follows:

$$D_m = \frac{\beta_m}{Q_d . \delta_{us}} \int dE \tag{3}$$

where, δ_{us} is the ultimate deflection from reversal cyclic loading tests; Q_d is calculated nominal strength; dE is incremental absorbed hysteric energy and β_m is a model parameter. The corresponding value of β_m for each specimen is calculated by setting D_m equal to 1.0 at failure (0.151 and 0.175 for Specimen EX-1.3 and In-13, respectively).

Fig. 18 compares the calculated damage index for test specimens during the first loading phase. As expected, Specimen In-1.3 constantly exhibited higher damage index compared to Specimen Ex-1.3.

3.7 Performance under service loading

To measure performance of the specimens under service loading after withstanding severe lateral displacements, one load-controlled cycle with an amplitude equal to service load was applied after each loading step passed the 2% drift ratio. Generally, service loads in the beams are applied in gravity direction in real structures while the test set-up used in this program only allowed the application of lateral displacements to the upper tip of the column. Therefore, in order to apply service bending moments to the main beams in the test specimens, service loading condition was calculated as the corresponding lateral load at the tip of the column that exerts bending moments equal to service condition into the main beams.

Fig. 19(a) shows the maximum column tip displacement at each of the service loading cycles as a ratio of the column tip displacement when the service load condition was reached for the first time (2% and 0.8% drift ratios in Specimens Ex-1.3 and In-1.3, respectively). The performance of Specimen Ex-1.0 is also included in the graphs for comparison. According to the graph (Fig. 19(a)), the performance of the specimens under service loadings shows direct relationship to the reinforcement ratio of the

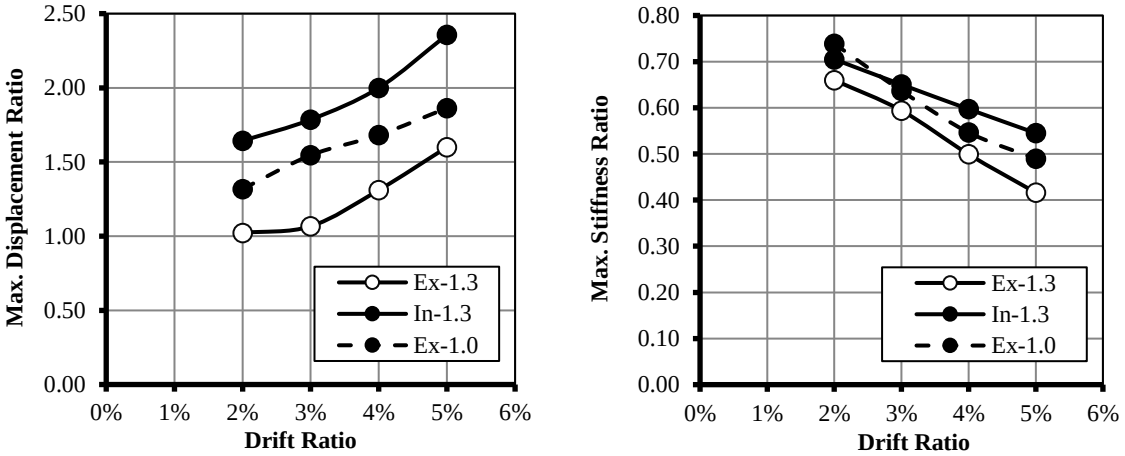

(a) Maximum displacement ratio (b) Lateral stiffness ratio

Fig. 19 Performance of test specimens during service load stage

main beams. The higher the reinforcement ratio, the lower the increase in the lateral displacement ratio during service loading cycles.

The lateral stiffness of the specimens during each service loading cycle is illustrated in Fig. 19(b) as a ratio of the lateral stiffness of the specimens during the first cyclic loading step (0.8% drift ratio). The lateral stiffness was calculated as the slope of the straight line connecting the maximum positive and negative points in the hysteresis diagram during the service loading cycles. Comparing the behavior of Specimens Ex-1.0 and Ex-1.3 illustrates that the increase in shear stress ratio increases the stiffness degradation of beam-column joints. This is due to the higher concrete damage in the joint area because of higher joint shear stresses.

Moreover, comparing the interior and the exterior specimens with equal joint shear stress ratios (Ex-1.3 and In-1.3) indicates that the interior beam-column joints exhibit lower stiffness degradation compared to their exterior counterparts. This is attributed to the better confinement provided to the joint area by the main beams in interior beam-column joints compared to the exterior ones.

4. Conclusions

Based on the results obtained from the test specimens, the following conclusions can be made:

- The exterior beam-column joint (Ex-1.3) was able to reach its maximum nominal lateral load capacity resulting in joint shear stress of $1.3\sqrt{f'_c}$. Therefore, it is concluded that exterior GFRP-RC beam-column joints with lateral beams can withstand joint shear stress ratios of 1.3.
- Both test specimens (In-1.3 and Ex-1.3) were able to reach their nominal capacity during the first loading phase (up to 5% drift ratio) without exhibiting significant concrete damage. Therefore, it is concluded that GFRP-RC moment-resisting frames can withstand significant lateral deformations and still maintain their original condition up to an acceptable level. This characteristic can significantly reduce the repair costs of moment-resisting frames after an earthquake event.
- During the second loading phase, both test specimens showed linear behavior up to 5% lateral drift ratios. The exterior beam-column joint (Ex-1.3) was able to reach the nominal capacity for the second time during the second loading phase while the interior specimen with the same magnitude of joint shear stress (In-1.3) was not able to reach its nominal capacity. This was attributed to the effect of longitudinal reinforcement in the main beams on the confinement of concrete core, which improved the performance of Specimen Ex-1.3.
- Both test specimens failed due to gradual decrease in lateral load carrying capacity (more than 25%) without brittle failure or sudden rapture of the GFRP bars. Therefore, it is concluded that GFRP-RC beam-column joints can be designed to prevent sudden and catastrophic failure.
- At failure, significant damage was observed in the joint area of the exterior specimen (Ex-1.3), while the concrete damage in the interior specimen (In-1.3) was concentrated in the beam area in the vicinity of the joint. This was attributed to the better confinement provided to the joint area in the interior specimen by the main beams, which increased the shear capacity of the joint.
- The maximum strain measured in the joint stirrups did not exceed the limit suggested by the CSA/S806-12 (CSA 2017) up to 5% drift ratio during both loading phases. This indicates that the amount of lateral reinforcement suggested by CSA/S806-12 (CSA 2017) for confinement of columns in seismic regions is sufficient to withstand a joint shear stress of $1.3\sqrt{f'_c}$ in exterior and interior GFRP-RC beam-column joints.
- Test results showed that the longitudinal reinforcement ratio of the main beams had a significant effect on the maximum strain observed in the longitudinal bars during an earthquake. This should be taken into account to prevent rupture of the longitudinal bars by providing sufficient margin between the maximum expected strain in the bars and their tensile strain capacity.
- Test results indicated that the secondary moments,

calculated considering the column load remains vertical, resulted in a 19 and 18% increase in the bending moment in columns of Specimens Ex-1.3 and In-1.3, respectively, at 5% drift ratio.

• Measured cumulative energy dissipation of the test specimens indicated that interior beam-column joints dissipate more energy than their exterior beam-column counterparts with equal magnitude of joint shear stress. This is attributed to the fact that, compared to exterior ones, interior beam-column joints have more concrete, which increases the area of damage concrete (cracked or crushed) that represents the main source of energy dissipation in GFRP-RC beam-column joints.

• Investigating the performance of the test specimens under service loading condition indicated that the reinforcement ratio of the main beams have significant effect on the performance of the specimens in terms of deformations under service loads. Higher reinforcement ratios resulted in less deformation increase under service loads after undertaking seismic loading cycles.

Acknowledgements

The authors wish to express their sincere gratitude for the financial support received from the Natural Sciences and Engineering Council of Canada (NSERC) and the University of Manitoba Graduate Fellowship (UMGF). The assistance received from the technical staff of the W. R. McQuade Structures Laboratory at the University of Manitoba is acknowledged.

References

ACI-ASCE Committee 352 (2002), Recommendation for Design of Beam-Column Connections in Monolithic Reinforced Concrete Structures, ACI 374.1-05, American Concrete Institute, Farmington Hills, Detroit, Michigan.

American Concrete Institute (ACI) Committee 374 (2005), Acceptance Criteria for Moment Frames Based on Structural Testing and Commentary, ACI 374.1-05, American Concrete Institute, Farmington Hills, Detroit, Michigan.

Brown, V. and Bartholomew, C. (1993), "FRP reinforcing bars in reinforced concrete members", *ACI Mater. J.*, **90**(1), 34-39.

Canadian Standard Association (CSA) (2014), Design of Concrete Structures, CAN/CSA A23.3-14, Canadian Standard Association, Ontario, Canada.

Canadian Standards Association (CSA) (2017), Design and Construction of Building Structures with Fibre Reinforced Polymers, CAN/CSA-S806-12, Canadian Standards Association, Ontario, Canada.

Ehsani, M. and Wight, J. (1985), "Exterior reinforced concrete beam-to-column connections subjected to earthquake", *ACI J. Proc.*, **82**(4), 492-499.

Esfandiari, J. and Latifi, M.K. (2019), "Numerical study of progressive collapse in reinforced concrete frames with FRP under column removal", *Adv. Concrete Constr.*, **8**(3), 165-172. https://doi.org/10.12989/acc.2019.8.3.165.

Esfandiari, J. and Soleimani, E. (2018), "Laboratory investigation on the buckling restrained braces with an optimal percentage of microstructure, polypropylene and hybrid fibers under cyclic loads", *Compos. Struct.*, **203**, 585-598. https://doi.org/10.1016/j.compstruct.2018.07.035.

Esfandiari, S. and Esfandiari, J. (2016), "Simulation of the behavior of RC columns strengthen with CFRP under rapid loading", *Adv. Concrete Constr.*, **4**(4), 14. https://doi.org/10.12989/acc.2016.4.4.319.

Fukuyama, H., Masuda, Y., Sonobe, Y. and Tanigaki, M. (1995), "Structural performances of concrete frame reinforced with FRP reinforcement", *Non-Metallic (FRP) Reinforcement for Concrete Structures, Proc., Second Int. RILEM Symp. (FRPRCS-2)*, E &FN Spon, London, 275-286.

Ghomi, S.K. and El-Salakawy, E. (2016), "Seismic performance of GFRP-RC exterior beam-column joints with lateral beams", *J. Compos. Constr.*, ASCE, **20**(1), 11. https://doi.org/10.1061/(ASCE)CC.1943-5614.0000582.

Guerin, M., Mohamed, H.M., Benmokrane, B., Shield, C.K. and Nanni, A. (2018), "Effect of glass fiber-reinforced polymer reinforcement ratio on axial-flexural strength of reinforced concrete columns", *ACI Struct. J.*, **115**(4), 17. https://doi.org/10.14359/51701279.

Hanson, N. and Connor, H. (1967), "Seismic resistance of reinforced concrete beam-column joints", *J. Struct. Div., Proc. Am. Soc. Civil Eng.*, ASCE, **93**(ST5), 533-560.

Hasaballa, M. and El-Salakawy, E. (2016), "Shear capacity of Type-2 exterior beam-column joints reinforced with GFRP bars and stirrups", *J. Compos. Constr.*, ASCE **20**(2), 13. https://doi.org/10.1061/(ASCE)CC.1943-5614.0000609.

Ju, M., Park, C. and Kim, Y. (2017), "Flexural behavior and a modified prediction of deflection of concrete beam reinforced with ribbed GFRP bars", *Comput. Concrete*, **19**(6), 631-639. https://doi.org/10.12989/cac.2017.19.6.631.

Kakaletsis, D.J. (2016), "Comparative experimental assessment of seismic rehabilitation with CFRP strips and sheets on RC frames", *Earthq. Struct.*, **10**(3), 613-628, https://doi.org/10.12989/eas.2016.10.3.613.

Karayannis, C.G. and Golias, E. (2018), "Full scale tests of RC joints with minor to moderate seismic damage repaired using C-FRP sheets", *Earthq. Struct.*, **15**(6), 617-627, https://doi.org/10.12989/eas.2018.15.6.617.

Kim, J. and LaFave, J. (2007), "Key influence parameters for the joint shear behaviour of Reinforced Concrete (RC) beam-column connections", *Eng. Struct.*, **29**(10), 2523-2539. https://doi.org/10.1016/j.engstruct.2006.12.012.

Le-Trung, K., Lee, K., Shin, M. and Lee, J. (2013), "Seismic performance evaluation of RC beam-column connections in special and intermediate moment frames", *J. Earthq. Eng.*, **17**(2), 187-208. https://doi.org/10.1080/13632469.2012.730116.

Liang, J., Yu, D., Wang, J. and Yi, P. (2016), "Mechanical properties of concrete beams reinforced with CFRP prestressed prisms under reverse cyclic loading", *Earthq. Struct.*, **11**(2), 315-326. https://doi.org/10.12989/eas.2016.11.2.315.

Mady, M., El-Ragaby, A. and El-Salakawy, E. (2011), "Seismic behavior of beam-column joints reinforced with GFRP bars and stirrups", *J. Compos. Constr.*, ASCE, **15**(6), 875-886. https://doi.org/10.1061/(ASCE)CC.1943-5614.0000220.

Mirmiran, A. and Shahawy, M. (1997), "Behavior of concrete columns confined by fiber composites", *J. Struct. Eng.*, ASCE, **123**(5), 583-590. https://doi.org/10.1061/(ASCE)0733-9445(1997)123:5(583).

National Research Council of Canada (NRCC) (2015), National Building Code of Canada, National Research Council of Canada, Ottawa, Ontario, Canada.

Park, R. and Ang, A.H.S. (1985), "Reinforced concrete beam-column joints under seismic actions", *ACI J. Proc.*, **75**(11), 585-593.

Paulay, T., Park, R. and Priestley, M.J. (1978), "Mechanistic seismic damage model for reinforced concrete", *Struct. Eng.*, ASCE, **111**(4), 722-739. https://doi.org/10.1061/(ASCE)0733-

9445(1985)111:4(722).
Pessiki, S., Harries, K.A., Kenstner, J.T., Sause, R. and Ricles, J. (2001), "Axial behavior of reinforced concrete columns confined with FRP jackets", *J. Compos. Constr.*, ASCE, **5**(4), 237-245. https://doi.org/10.1061/(ASCE)1090-0268(2001)5:4(237).
Pultrall Inc., GFRP Specification Guide, Available at http://www.vrodcanada.com/product-data/gfrp-specification-guide.
Said, A.M. and Nehdi, M.L. (2004), "Use of FRP for RC frames in seismic zones: Part II. Performance of steel-free GFRP-reinforced beam-column joints", *Appl. Compos. Mater.*, **11**, 227-245. https://doi.org/10.1023/B:ACMA.0000035480.85721.b5.
Schoeck Canada Inc., Technical Information Sheet, Available at https://www.schoeck.com/en/download/eyJjYXRlZ29yeSI6eyI3Ijo3fX0.
Sharbatdar, M.K., Saatcioglu, M. and Benmokrane, B. (2011), "Seismic flexural behavior of concrete connections reinforced with CFRP bars and frids", *Compos. Struct.*, **93**, 11. https://doi.org/10.1016/j.engstruct.2010.04.020.
Sumathi, A. and Vignesh, S. (2017), "Study on behavior of RCC beams with externally bonded FRP members in flexure", *Adv. Concrete Constr.*, **5**(6), 14. https://doi.org/10.12989/acc.2017.5.6.625.
Tavassoli, A. and Sheikh, S. (2017), "Seismic resistance of circular columns reinforced with steel and GFRP", *J. Compos. Constr.*, ASCE, **21**(4), 13. https://doi.org/10.1061/(ASCE)CC.1943-5614.0000774.
Tavassoli, A., Liu, J. and Sheikh, S. (2015), "Glass fiber-reinforced polymer-reinforced circular columns under simulated seismic loads", *ACI Struct. J.*, **112**(1), 12. https://doi.org/10.14359/51687227.
Tobbi, H., Farghaly, A.S. and Benmokraine, B. (2012), "Concrete columns reinforced longitudinally and transversally with glass fibre-reinforced polymer bars", *ACI Struct. J.*, **109**(4), 10. https://doi.org/10.14359/51686630.
Tobbi, H., Farghaly, A.S. and Benmokrane, B. (2014), "Strength model for concrete columns reinforced with fiber-reinforced polymer bars and ties", *ACI Struct. J.*, **111**(4), 789-798.
Tobbi, H., Farghaly, A.S. and Benmokrane, B. (2014), "Strength model for concrete columns reinforced with fiber-reinforced polymer bars and ties", *ACI Struct. J.*, **111**(4), 789-798. https://doi.org/10.14359/51686630.

CC